Atmos. Chem. Phys. Discuss., 15, 10593–10628, 2015
www.atmos-chem-phys-discuss.net/15/10593/2015/
doi:10.5194/acpd-15-10593-2015

Atmospheric Chemistry and Physics Discussions

A PV-based determination of the transport barrier in the Asian summer monsoon anticyclone

F. Ploeger, C. Gottschling, S. Griessbach, J.-U. Grooß, G. Günther, P. Konopka, R. Müller, M. Riese, F. Stroh, J. Ungermann, B. Vogel, and M. von Hobe

Institute for Energy and Climate research: Stratosphere (IEK–7), Forschungszentrum Jülich, Jülich, Germany

Received: 20 February 2015 – Accepted: 21 March 2015 – Published: 13 April 2015

Correspondence to: F. Ploeger (f.ploeger@fz-juelich.de)

Published by Copernicus Publications on behalf of the European Geosciences Union.

Abstract

The Asian summer monsoon provides an important pathway of tropospheric source gases and pollution into the lower stratosphere. This transport is characterized by deep convection and steady upwelling, combined with confinement inside a large-scale anticyclonic circulation in the upper troposphere and lower stratosphere (UTLS). In this paper, we show that a barrier to horizontal transport along the 380 K isentrope in the monsoon anticyclone can be determined from the potential vorticity (PV) field, following the polar vortex criterion by Nash et al. (1996). Due to large dynamic variability of the anticyclone, the corresponding maximum in the PV gradient is weak and additional constraints are needed (e.g., time averaging). Notwithstanding, PV contours in the monsoon anticyclone agree well with contours of trace gas mixing ratios (CO, O_3) and mean age from model simulations with a Lagrangian chemistry transport model (CLaMS) and MLS satellite observations. Hence, the PV-based transport barrier reflects the separation between air inside the anticyclone core and the background atmosphere well. For the summer season 2011 we find an average PV value of 3.6 PVU for the transport barrier in the anticyclone on the 380 K isentrope.

1 Introduction

An efficient pathway for anthropogenic pollution and tropospheric source gases into the stratosphere is linked to the Asian summer monsoon, as has been shown from satellite observations of HCN (Randel et al., 2010). Upward transport in the monsoon is caused by frequent high-reaching convection (e.g., Tzella and Legras, 2011; Bergman et al., 2012) and slower steady upwelling at higher levels around the tropopause. In the upper troposphere and lower stratosphere (UTLS), strictly in the Tropical Tropopause Layer TTL (e.g., Fueglistaler et al., 2009), the Asian monsoon is characterized by a large-scale anticyclonic circulation system, the linear response to strong diabatic heating at low levels (Gill, 1980). The anticyclonic circulation confines the upward transported

ACPD
15, 10593–10628, 2015

air and isolates it, to some degree, from its surroundings. This confinement leads to positive anomalies of tropospheric trace gases (e.g., CO, HCN, H_2O) and to negative anomalies of stratospheric trace gases (e.g., ozone) in the anticyclone (e.g., Randel and Park, 2006; Park et al., 2006, 2008; James et al., 2008; Bian et al., 2012).

For an improved understanding of the pollution transport by the monsoon, understanding the confinement of trace gases within the anticyclone is crucial. However, the Asian monsoon anticyclone is characterized by large dynamic variability (Garny and Randel, 2013), characterized by strong east–west displacements (Krishnamurti et al., 1973), frequent shedding of small-scale eddies (Hsu and Plumb, 2000; Popovich and Plumb, 2001) and even splits. Moreover, strong diabatic heating processes play a role in the monsoon and, consequently, PV is not well conserved (e.g., Holton, 1992). For these reasons, the confinement of air inside the Asian monsoon anticyclone appears much weaker than in the polar vortex, and it turns out to be very challenging to locate a barrier to horizontal transport (Garny and Randel, 2013). However, that such a transport barrier exists, at least to some degree, is reflected in the observed trace gas anomalies within the anticyclone. To date, simplified criteria have been adopted to define this transport barrier and to separate the core region of the anticyclone from its surroundings. These criteria are commonly based on the positive geopotential height (GPH) anomaly or the negative PV anomaly in the monsoon region and assume a fixed GPH (on a fixed pressure level) or PV value to represent the transport barrier (e.g., Randel and Park, 2006; Bergman et al., 2013).

In this paper, we present a physically motivated criterion to deduce the transport barrier in the Asian monsoon anticyclone. This criterion is closely related to a well-established methodology based on PV gradients on isentropic surfaces, which has been originally developed for the polar vortex (Butchart and Remsberg, 1986; Nash et al., 1996). In fact, the method relies on the characteristics of PV being an approximately conserved quantity, such that a maximum in the PV gradient on an isentrope reflects the existence of a barrier to transport.

ACPD
15, 10593–10628, 2015

We introduce the data and model used in Sect. 2. In Sect. 3 we motivate the use of PV as a basis for deducing the anticyclone transport barrier, by comparing PV to simulated and observed trace gas distributions (CO, O_3) in the Asian monsoon region. The criterion for deducing the transport barrier is presented in Sect. 4, and validated by comparison to simulated CO, ozone and mean age in Sect. 5. We finally discuss our results and conclude.

2 Data and model

Meteorological fields to characterize the Asian monsoon anticyclone are taken from European Centre for Medium-Range Weather Forecasts (ECMWF) ERA-Interim reanalysis. ERA-Interim covers the period from 1979 until present, assimilating observational data from several sources to provide a reliable state of the atmosphere (for details, see Dee et al., 2011). We interpolated the data on a $1^\circ \times 1^\circ$ horizontal grid and on potential temperature (θ) levels in the vertical. The presented analysis focusses on the summer season (June–August, JJA) 2011 and on the 380 K isentropic surface, which is a characteristic level for the Asian upper-level anticyclone in the upper troposphere and lower stratosphere (UTLS). Note that in the tropics 380 K is close to the 100 hPa isobaric surface, which has been used in several studies to analyse transport in the Asian monsoon anticyclone (e.g., Randel and Park, 2006; Bergman et al., 2013).

The most relevant meteorological fields for this study are Ertel's potential vorticity (PV), the circulation (Γ), and the Montgomery stream function (M). PV is calculated from the horizontal winds (e.g., Holton, 1992)

$$\mathrm{PV} = \sigma^{-1}(\zeta + f), \tag{1}$$

with ζ the relative vorticity, $f = 2\Omega \sin\phi$ the Coriolis parameter, and $\sigma = -g^{-1}\partial_\theta p$ the isentropic mass density (p pressure, ϕ latitude, g acceleration due to gravity). PV is a particularly well suited quantity for characterizing barriers to transport. In the absence of friction and diabatic processes the PV of an air parcel is conserved following its

ACPD
15, 10593–10628, 2015

motion (e.g., Holton, 1992), and thus regions of enhanced PV gradients are indicative for suppressed transport (transport barriers). This fact has been used by Nash et al. (1996) to deduce the transport barrier for the polar vortex, based on the gradient of PV along an isentropic surface.

A related quantity, characterizing fluid rotation, is the circulation Γ along a closed contour S (here, on an isentrope)

$$\Gamma = \oint_S \mathrm{d}\boldsymbol{s} \cdot \boldsymbol{v} = \int_A \mathrm{d}a\, \zeta\,, \tag{2}$$

with A the area enclosed by the contour S and $\boldsymbol{v} = (u, v)$ the horizontal wind on an isentropic surface ($\mathrm{d}\boldsymbol{s}$ and $\mathrm{d}a$ represent line and area elements). Therefore, cyclonic flow is characterized by positive circulation, while anticyclonic flow is characterized by negative circulation.

The Montgomery stream function $M = c_p T + \Phi$ (with Φ geopotential, T temperature, and c_p the specific heat at constant pressure) is the isentropic analogue of geopotential, which is frequently used to characterize the monsoon anticyclone (Randel and Park, 2006; Bergman et al., 2013). Under geostrophic approximations the horizontal flow on an isentrope is along contours of constant M (e.g., Holton, 1992).

Due to the anticyclonic nature of the upper-level circulation, the Asian monsoon in the UTLS is characterized by strongly negative, anomalously low PV (see Fig. 1), and anomalously high Montgomery stream function values. To the north, the anticyclone is bounded by the subtropical westerly jet, to the south by the equatorial easterly jet. Furthermore, the monsoon region is characterized by an elevated thermal tropopause which, from a climatological point of view, exceeds the zonal mean tropopause by more than 1 km (Fig. 1), corresponding to ≈ 20 K in potential temperature.

To confirm the deduced location of the transport barrier, which will be based on PV, we consider different trace gas species (carbon monoxide CO, ozone O_3) and mean age of air from model simulations with the Chemical Lagrangian Model of the Stratosphere CLaMS (McKenna et al., 2002a, b; Konopka et al., 2007), driven by ERA-

ACPD
15, 10593–10628, 2015

Interim meteorological data. CLaMS is a Lagrangian chemistry transport model (CTM), based on 3-D forward trajectories, with an additional parameterization for small-scale mixing, which depends on the deformation in the large-scale flow. Vertical transport in the model is purely diabatic above about 300 hPa, with the total diabatic heating rates taken from ERA-Interim forecast data. For further details about this specific CLaMS simulation, and in particular about the representation of CO, O_3 and mean age in the model, see Pommrich et al. (2014).

3 Trace gas confinement in the anticyclone and PV

Figure 2a and b shows the distributions of CLaMS CO and ozone in the monsoon region on the 380 K isentrope, exemplarily for one day during summer (6 July 2011). Clearly visible is the positive anomaly of the tropospheric tracer CO and the negative anomaly of the stratospheric tracer ozone in the monsoon, characteristic for strong tropospheric impact and confinement within the anticyclone. Note that extratropical stratospheric air is advected around the eastern flank of the anticyclone, transporting CO-poor and ozone-rich air equatorwards. This transport has recently been shown to strongly affect the ozone seasonality in the tropics (Konopka et al., 2010; Ploeger et al., 2012; Abalos et al., 2013). Furthermore, poleward transport of CO-rich air affects the trace gas composition of the lowermost stratosphere and crucially depends on the CO lifetime (e.g., Hoor et al., 2010). To create a similar map from ozone measurements, we bin ozone observations from the Microwave Limb Sounder (MLS) instrument onboard the Aura satellite (Livesey et al., 2008) between 4 and 8 July 2011 (using version 3.3 data), in order to obtain sufficiently dense observations (Fig. 2c). Lower ozone mixing ratios in the model compared to MLS are likely related to the broad satellite averaging kernel and the zero mixing ratio lower boundary condition at the surface in the model (Pommrich et al., 2014). However, the patterns of the low ozone anomaly in the monsoon reliably agree between model and simulations (note also the five-day average for the satellite data).

ACPD
15, 10593–10628, 2015

Overlaid to the trace gas mixing ratios in Fig. 2 are contours of PV and Montgomery stream function. Both meteorological quantities show strong anomalies within the monsoon. However, when compared to the trace gas mixing ratio contours the PV contours agree much better than the Montgomery stream function contours, in particular for small-scale variations. Even the separation of a smaller eddy to the east of the main anticyclone is well reflected in the PV distribution. These small scale eddies, frequently shedded from the main anticyclone, have the potential to transport air masses with elevated mixing ratios of tropospheric trace gases (e.g., CO, H_2O) rapidly into the middle and high latitude lower stratosphere (e.g., Ploeger et al., 2013; Vogel et al., 2014). A close relation between the distributions of CO and PV in the monsoon has already been found by Garny and Randel (2013). For these reasons, we use PV as a basis for defining a criterion for the transport barrier in the Asian monsoon.

Motivated by the work of Butchart and Remsberg (1986) and Nash et al. (1996) that the transport barrier of the polar vortex is characterized by particularly steep gradients of conserved tracers, we map MLS and CLaMS ozone vs. potential vorticity (Fig. 3). This mapping has been carried out by binning all data from the Asian monsoon region at 380 K with respect to potential vorticity (bin size 0.1 PVU). Figure 3 shows that, despite the offset between CLaMS and MLS ozone mentioned above, there is agreement in the main structure with low ozone in the core of the anticyclone (at low PV values) and higher mixing ratios towards higher PV. In particular, there is evidence from model and observations for a two-step increase of ozone mixing ratios, resulting in two separate maxima in the gradient of ozone with respect to PV. The stronger maximum around 7 PVU is related to the transport barrier at the subtropical jet (Kunz et al., 2011). The secondary maximum occurs around 4 PVU. In the following, we will provide evidence that this secondary maximum may be interpreted as the transport barrier of the Asian monsoon anticyclone (red line shows the transport barrier PV value, objectively determined using the criterion derived in the following section).

ACPD
15, 10593–10628, 2015

4 A PV-gradient criterion for the Asian monsoon

Motivated by the good agreement between the PV and trace gas varability in the monsoon region (Fig. 2) and the fact that PV is an approximately conserved quantity, we follow the approach of Nash et al. (1996) for deducing a transport barrier. Originally, this approach has been applied to the polar vortex. Nash et al. (1996) defined the transport barrier of the vortex edge as the location of the largest (isentropic) change in PV, with the additional constraint of close proximity to a strong zonal jet. Recently, Kunz et al. (2011) deduced the location of the transport barrier of the subtropical jet using an analogous approach.

In a first step, we restrict all fields to a region including the monsoon anticyclone, which we define as $10^\circ\,\mathrm{N} \le \phi \le 60^\circ\,\mathrm{N}$ and $-10^\circ\,\mathrm{E} \le \lambda \le 160^\circ\,\mathrm{E}$ (ϕ latitude, λ longitude) to eliminate the interfering influence of low PV values near the equator. The PV distribution on 6 July 2011 within this region is exemplarily shown in Fig. 5a (top). A similar definition of the Asian mosoon area has been used by Garny and Randel (2013). The chosen latitude/longitude range includes the anticyclone for all days during summer 2011. Slight variations to this range cause no significant change of our results.

In analogy to Nash et al. (1996), we define a monsoon-centered equivalent latitude (ϕ_{eq}, in the following) of a given PV contour in the anticyclone as the latitude of a circle around the North pole enclosing the same area, as illustrated in Fig. 4 (here, the 4 PVU contour is mapped to $\phi_{\mathrm{eq}} = 65^\circ$). Hence, for a PV contour enclosing an area A, the equivalent latitude is defined by $A = 2\pi r_{\mathrm{E}}^2 (1 - \sin\phi_{\mathrm{eq}})$, with r_{E} the Earth's radius. Consequently, the center of the monsoon occurs at a monsoon equivalent latitude of 90°, corresponding to the location of minimum PV. In this sense, PV and equivalent latitude are related to each other, exhibiting a unique functional dependence $\mathrm{PV}(\phi_{\mathrm{eq}})$ as shown in Fig. 5a (bottom). As already noted above, PV increases monotonically from low values in the center of the anticyclone to higher values at its edge.

For 6 July 2011, the gradient of PV with respect to ϕ_{eq}, namely $\partial\mathrm{PV}/\partial\phi_{\mathrm{eq}}$, shows no clear maximum indicative for the anticyclone transport barrier, besides the maxi-

ACPD
15, 10593–10628, 2015

mum around 50° equivalent latitude (about 7–8 PVU) related to the transport barrier of the subtropical jet (Kunz et al., 2011). The absence of a clear secondary maximum, representing the anticyclone transport barrier, has recently been attributed to the large dynamical varibility of the anticyclone (Garny and Randel, 2013). However, if this variability is damped by averaging the PV field over a time window of 3 days between 5 and 7 July 2011, a clear secondary maximum in the PV gradient emerges around 65° equivalent latitude (Fig. 5b, bottom). In the following, we interprete this maximum as the transport barrier of the Asian monsoon anticyclone, and show its physical significance by comparison to trace gas distributions in Sect. 5.

To calculate the time averaged PV for different dates we use a variable time window. Therefore, we define an optimal window for each date as the smallest number of days (±3 days at most) such that the PV-gradient maximum exceeds the adjacent minima by 30 %. Figure 6 illustrates this procedure for the example of the 6 July 2011, confirming that for this date a ±1 day average (3 day time window) results in the clearest gradient maximum. If the time window is chosen too large (e.g., ±3 days in Fig. 6), the maximum in the PV gradient degrades again because different dynamical conditions contribute to the average. For that reason, we average maximum over 7 days (given date ±3 days). Notably, for some dates no time averaging is necessary to determine a PV-gradient maximum.

We apply an additional constraint to exclude the subtropical jet from the calculation, which generally shows much larger PV-gradient values than the anticyclone transport barrier. Empirically, for the summer 2011 a PV-limit of 5 PVU reliably separates the monsoon transport barrier from the subtropical jet at 380 K, as illustrated in Fig. 5b for 6 July. A physical motivation for this constraint can be deduced from the horizontal circulation (also averaged over ±1 day, see Fig. 7), as described in the following. Necessarily, the anticyclone transport barrier is located within the region of anticyclonic motion (negative relative vorticity), and hence in the equivalent latitude range of decreasing circulation. Consequently, the PV-gradient maximum of the anticyclone transport barrier needs to be located at equivalent latitudes lower than the minimum

ACPD
15, 10593–10628, 2015

circulation (4.8 PVU in Fig. 7). This circulation constraint generally excludes the subtropical jet from the transport barrier calculation. For simplicity, we use 5 PVU as an upper PV-limit for the transport barrier calculation at 380 K in the following, which is a good approximation of the circulation minimum. Note in addition that the second derivative of the circulation with respect to equivalent latitude $\partial^2\Gamma/\partial\phi_{eq}^2$ is related to the first derivative of PV (see Eq. 2). Therefore, the transport barrier defined from the maximum PV gradient can be approximated by the maximum in the second derivative of Γ (see Fig. 7, bottom), providing a consistency check of our procedure.

To summarize, the minimum circulation (approximately 5 PVU) defines the *anticyclone boundary*. The *anticyclone transport barrier* is then calculated from the time-averaged PV field as the maximum PV gradient at PV values larger than 5 PVU. The procedure is illustrated in Fig. 8, and generally results in a well defined PV value (e.g., 4 PVU for 6 July 2011, see Fig. 5b) characterizing the transport barrier for the Asian monsoon anticyclone for most days between about mid June and mid August 2011. For some days during the summer season, however, no clear maximum emerges in the PV-gradient even after averaging over a few days (see also Fig. 11), likely related to enhanced dynamic variability of the anticyclone during these days (compare Garny and Randel, 2013).

5 PV-based transport barrier and relation to trace gases

To investigate whether the diagnosed transport barrier is physically meaningful, in the sense of separating air masses of different chemical characteristics, we compare it to simulated CO in the Asian monsoon region. Figure 9 shows PV and CO maps at 380 K for the 6, 9, 12, 15, 18 and 21 July 2011, overlaid with the PV contours of the transport barrier (thick white), as deduced for each date following the procedure described in Sect. 4. First, the barrier calculated from the time averaged fields results in reasonable PV values also when compared to the instantaneous PV maps on the particular days.

ACPD
15, 10593–10628, 2015

Second, in the CO distributions the diagnosed barrier separates the high mixing ratios in the center of the anticyclone from the lower values around.

The sequence of plots in Fig. 9 illustrates the large variability of the anticyclone, with frequent shedding of smaller scale eddies (9 July) and even splits of the anticyclone (21 July). Also for days of particularly large variability the diagnosed barrier separates the core region of the anticyclone, characterized by high CO mixing ratios, well from its surroundings. Even the shedding of the smaller eddy and the vortex split are reflected in the transport barrier.

To investigate more quantitatively to what degree the transport barrier deduced from PV is reflected in the CO distribution, we apply the barrier calculation to CO, exemplarily for 6 July 2011. Therefore, we restrict the CO field to the monsoon region, average over ±1 days (5–7 July 2011), transform to PV-based monsoon centered equivalent latitude ϕ_{eq}, restrict to the anticyclonic region and calculate the PV value of the maximum CO gradient $\partial CO/\partial \phi_{eq}$. Figure 10a shows that a clear CO-gradient maximum emerges around 65°, equivalent to a PV value of 4 PVU, in agreement with the transport barrier deduced from the maximum PV-gradient. Similarly, distributions of simulated ozone and mean age of air reflect the PV-based transport barrier within the Asian monsoon region (Fig. 10b and c).

The PV-gradient based transport barrier for the Asian monsoon anticyclone has been calculated for all days between 20 June and 20 August 2011. Before this period and afterwards, almost no barrier could be found. Figure 11 (top) shows the evolution of the PV-gradient at 380 K over the summer season. Although the gradient maximum related to the anticyclone barrier appears weaker during some periods, it shows smooth subseasonal variability with higher PV values (around 4 PVU) at beginning of July and beginning of August and lower PV values (around 3.2 PVU) in mid July and mid August. Significant subseasonal dynamic variability of the Asian monsoon, occurring with a frequency of about 30 days, has been recently noted by Garny and Randel (2013). Only for a few days (end of June and beginning of August) no transport barrier could be deduced because no clear maximum in the PV gradient emerged. The evolution of the

ACPD
15, 10593–10628, 2015

CO-gradient over the summer season (Fig. 11b) shows a local maximum throughout most of the season, well coinciding with the PV-based transport barrier. Only after 15 August there is an additional structure in the CO distribution at PV values above 4 PVU, which is not reflected in the PV gradients.

At 380 K, the PV value at the determined transport barrier is generally found between about 3 and 4 PVU, and shows intraseasonal variability. The mean PV value of the transport barrier over the summer 2011 is 3.6 PVU (at 380 K), in very good agreement with the mean PV of the related CO-gradient maximum (Table 1). We calculated the transport barrier PV values also for summers 2012 and 2013 (see Table 1) and found some weak interannual variability which needs to be further investigated. Note that the interannual variability and model projected future changes of the Asian monsoon anticyclone are largely uncertain, hitherto (e.g., Kunze et al., 2010).

6 Transport barrier from trace gas mixing ratio PDF

To further increase the confidence in the existence of the PV-gradient transport barrier, we deduce the anticyclone transport barrier also from simulated CO using a different methodology and show its consistency with the PV-based results. Therefore, we follow Sparling (2000) and calculate the probability density function (PDF) of CLaMS simulated CO mixing ratios in the Asian monsoon region (10–60° N, 10° W–160° E) for a ±1 day time window around 6 July 2011 (Fig. 12). The PDF has been constructed after assigning the appropriate area-weighting to the data points. Mean CO monotonically decreases with increasing PV, with high CO inside the monsoon (coinciding with low PV) and low CO outside. Minima in the mixing ratio PDF indicate regions of suppressed horizontal transport (Sparling, 2000).

The PDF in Fig. 12 shows one minimum at CO mixing ratios around 35–40 ppbv, related to the subtropical jet, and a secondary minimum around 55 ppbv, related to the transport barrier inside the Asian monsoon anticyclone. From the PDF of PV values corresponding to CO mixing ratios around the minimum, we find a corresponding

ACPD
15, 10593–10628, 2015

PV value of 4.1 PVU, in good agreement to the 4 PVU emerging from the PV-gradient maximum (Fig. 12, bottom).

For 6 July, the CO PDF shows the anticyclone transport barrier even for the instantaneous distribution, without averaging over ±1 days (not shown). Note that the PDF approach is related to the PV-gradient method (e.g., Neu et al., 2003; Palazzi et al., 2011). Still, the comparison shows the robustness of the deduced transport barrier. The use of mixing ratio PDF's would offer a simple independent method to deduce the anticyclone transport barrier from satellite observations. Overall, the good agreement between the PV-gradient based, CO-gradient based and CO-PDF based approaches enhances our confidence in the physical meaningfulness of the deduced transport barrier estimates.

7 Discussion

Recently, Bergman et al. (2013) showed evidence for upward transport in the Asian monsoon occurring in a vertical conduit separated from the main anticyclone. Hence, it is not the anticyclone itself but this conduit which defines the most efficient pathway of polluted surface air to higher altitudes. However, as the air is released from the conduit at greater altitudes, it stays confined and chemically isolated, at least to some degree, inside the anticyclone, as shown from trace gas observations (e.g., Park et al., 2006, 2008). Therefore, a complete understanding of pollution transport from the boundary layer into the stratosphere requires understanding of the confinement inside the upper level anticyclone.

In this paper, we investigated to what extent meteorological fields and trace gas distributions reflect the existence of a barrier to (quasi-)horizontal transport along isentropic surfaces in the Asian monsoon anticyclone. We followed the methodology of Nash et al. (1996) and found a secondary maximum besides the subtropical jet maximum in the gradient of potential vorticity with respect to a monsoon centered equivalent latitude (related to the area enclosed within PV contours). We interpreted this PV-gradient

ACPD
15, 10593–10628, 2015

maximum as the transport barrier in the monsoon anticyclone. The PV-gradient based transport barrier in the monsoon anticyclone appears much weaker than the transport barrier at the edge of the polar vortex (Nash et al., 1996) and also weaker than the barrier at the subtropical jet (see Kunz et al., 2011), likely related to the large dynamic variability of the monsoon anticyclone. The anticyclone shows large displacements in east–west direction, frequent shedding of smaller-scale eddies and even splits during the monsoon season (Fig. 9), related to strong diabatic heating events (Garny and Randel, 2013). However, after refining the approach of Nash et al. (1996) by additional constraints (e.g., time averaging, restriction to anticyclone) a PV-gradient based transport barrier is deducible for the monsoon anticyclone in a layer around the tropopause (around 380 K). Below, at levels of the subtropical jet core around 360 K, the stronger jet to the north of the monsoon masks the existence of the anticyclone transport barrier (Garny and Randel, 2013). Figure 13 shows that the PV-gradient based transport barrier turns out to be clearest at the 380 K level, still detectable at 370 and 390 K, but becomes undetectable below (360 K) and above (400 K).

Note that the tropopause within the monsoon is located at particularly high altitudes (see Fig. 1). From this point of view, the diagnosed transport barrier can also be interpreted as a PV-based tropopause definition, separating air of more tropospheric character inside the anticyclone from air of more stratospheric character outside. Compared to the zonal mean, the tropopause is upward bulging in the monsoon anticyclone by about 20 K potential temperature (Fig. 1). This could explain the thin layer of a detectable transport barrier around 380 K, where air inside the anticyclone is tropospheric and surrounding air stratospheric.

The smooth evolution of the anticyclone transport barrier over the season (Fig. 11) enhances our confidence in its relation to a physical mechanism rather than simply to noise in the PV distribution. Furthermore, enhanced gradients in trace gas distributions (MLS observed O_3, and CLaMS simulated CO, O_3 and mean age) clearly demonstrate the existence of the PV-gradient based transport barrier. These enhanced trace gas gradients are reflected in corresponding minima in mixing ratio PDFs (Fig. 12).

ACPD
15, 10593–10628, 2015

The location probability for the region enclosed by the transport barrier ("anticyclone core region", in the following) is shown in Fig. 14. Presented is the local frequency of occurrence for PV values lower than the anticyclone barrier value, in units of percentage of days during summer 2011 (20 June to 20 August 2011). Clearly, the largest probability of being located inside the anticyclone core occurs around 70° E/30° N (above 80 % of the considered days). The whole region between about 25–40° N and 20–100° E is located within the anticyclone core for more than 50 % of the days. Note that the anticyclone location probability may show significant interannual variability which needs to be further studied.

Zhang et al. (2002) and Yan et al. (2011) found an enhanced probability for the anticyclone center (estimated as geopotential height maximum) to occur at longitudes of the Tibetan and the Iranian plateaus, resulting in a bimodal longitude occurrence frequency. Figure 14a shows no enhanced probability for the anticyclone to be located in these two regions. Inspection of daily PV maps shows that the area of lowest PV rotates clock-wise with the anticyclonic flow (not shown). Similar to a children's roundabout such a rotation would cause no preferred locations for the anticyclone in the horizontal plane (Fig. 14a). However, if projected onto the longitude axis, the anticyclone location probability indicates two weak maxima (Fig. 14a, bottom), located at about 55 and 85° E. Hence, the bimodality of the anticyclone longitude occurrence frequency appears to be related, at least partly, to the projection of the (anticyclonic) rotation onto the longitude axis.

Note that the large zonal extent of the anticyclone occurrence probability at 380 K in Fig. 14a is related to frequent eddy shedding events, with the above analysis not distinguishing between the main anticyclone and westward and eastward travelling eddies. Further note that at lower levels (e.g., at 360 K in Fig. 14b) the region of lowest PV values is more confined and located further eastward and southward above the Tibetan plateau and Northern India, in agreement with the existence of the vertical conduit proposed by Bergman et al. (2013).

ACPD
15, 10593–10628, 2015

Finally, the PV-based anticyclone transport barrier needs to be further verified using trace gas measurements. Unfortunately, high-resolution in-situ observations from the Asian monsoon region are lacking. Current satellite observations are often affected by high clouds in this region, and further their vertical resolution and horizontal spatial sampling is limited. Nonetheless, MLS ozone shows enhanced gradients coinciding with the PV value of the transport barrier (Fig. 3), providing evidence for the anticyclone transport barrier to exist. Further analysis of observations of sufficiently high resolution would be strongly desirable.

8 Conclusions

As shown by anomalies in several trace gas observations, the air inside the Asian monsoon anticyclone appears, at least to some degree, confined and isolated from its surroundings. Diagnosing the related transport barrier is crucial for quantifying the transport of tropospheric source gases into the UTLS. In this paper, we showed that the potential vorticity field reflects the existence of a barrier to horizontal transport between the anticyclone and its surroundings. Although the detection of the transport barrier is hampered by the large dynamic variability of the anticyclone and the proximity to the subtropical jet a refined PV-gradient criterion may be used to deduce the barrier within the Asian monsoon anticyclone, in a layer around 380 K. Therefore, we refined the criterion of Nash et al. (1996) and determine the anticyclone transport barrier from the PV-gradient maximum, after restricting the PV field to the monsoon region and averaging over a time window around the given date (summarized in Fig. 8). Comparison to simulated CO shows that the PV-gradient based transport barrier is meaningful in the sense of separating air masses of different chemical characteristics. The deduced PV values (e.g., 3.6 on average for 2011 at 380 K) offer a physically motivated criterion to separate the inner core of the anticyclone from the region around, crucial for the interpretation of trace gas observations and for model studies.

ACPD
15, 10593–10628, 2015

Acknowledgements. We thank Bernard Legras for advice, Nicole Thomas for programming support and the ECWMF for providing reanalysis data. F. Ploeger was funded by an HGF postdoc grant, and further thanks the HGF for supporting a research stay at the Laboratoire de Météorologie Dynamique of the École Normale Supérieure in Paris during which parts of this work had been carried out.

The article processing charges for this open-access publication were covered by a Research Centre of the Helmholtz Association.

References

Abalos, M., Ploeger, F., Konopka, P., Randel, W. J., and Serrano, E.: Ozone seasonality above the tropical tropopause: reconciling the Eulerian and Lagrangian perspectives of transport processes, Atmos. Chem. Phys., 13, 10787–10794, doi:10.5194/acp-13-10787-2013, 2013. 10598

Bergman, J. W., Jensen, E. J., Pfister, L., and Yang, Q.: Seasonal differences of vertical-transport efficiency in the tropical tropopause layer: on the interplay between tropical deep convection, large-scale vertical ascent, and horizontal circulations, J. Geophys. Res., 117, D05302, doi:10.1029/2011JD016992, 2012. 10594

Bergman, J. W., Fierli, F., Jensen, E. J., Honomichl, S., and Pan, L. L.: Boundary layer sources for the Asian anticyclone: regional contributions to a vertical conduit, J. Geophys. Res., 118, 2560–2575, 2013. 10595, 10596, 10597, 10605, 10607

Bian, J., Pan, L. L., Paulik, L., Vömel, H., Chen, H., and Lu, D.: In situ water vapor and ozone measurements in Lhasa and Kunming during the Asian summer monsoon, Geophys. Res. Lett., 39, L19808, doi:10.1029/2012GL052996, 2012. 10595

Butchart, N. and Remsberg, E. E.: The area of the stratospheric polar vortex as a diagnostic for tracer transport on an isentropic surface, J. Atmos. Sci., 43, 1319–1339, 1986. 10595, 10599

Dee, D. P., Uppala, S. M., Simmons, A. J., Berrisford, P., Poli, P., Kobayashi, S., Andrae, U., Balmaseda, M. A., Balsamo, G., Bauer, P., Bechtold, P., Beljaars, A. C. M., van de Berg, L., Bidlot, J., Bormann, N., Delsol, C., Dragani, R., Fuentes, M., Geer, A. J., Haimberger, L., Healy, S. B., Hersbach, H., Holm, E. V., Isaksen, L., Kallberg, P., Kohler, M., Matricardi, M.,

ACPD
15, 10593–10628, 2015

McNally, A. P., Monge-Sanz, B. M., Morcrette, J. J., Park, B. K., Peubey, C., de Rosnay, P., Tavolato, C., Thepaut, J. N., and Vitart, F.: The ERA-Interim reanalysis: configuration and performance of the data assimilation system, Q. J. Roy. Meteor. Soc., 137, 553–597, doi:10.1002/qj.828, 2011. 10596

Fueglistaler, S., Dessler, A. E., Dunkerton, T. J., Folkins, I., Fu, Q., and Mote, P. W.: Tropical tropopause layer, Rev. Geophys., 47, RG1004, doi:10.1029/2008RG000267, 2009. 10594

Garny, H. and Randel, W. J.: Dynamic variability in the Asian monsoon anticyclone observed in potential vorticity and correlations with tracer distributions, J. Geophys. Res., 118, 13421–13433, 2013. 10595, 10599, 10600, 10601, 10602, 10603, 10606

Gill, A. E.: Some simple solutions for heat-induced tropical circulation, Q. J. Roy. Meteor. Soc., 106, 447–462, 1980. 10594

Holton, J. R.: An Introduction to Dynamic Meteorology, Academic Press, London, 1992. 10595, 10596, 10597

Hoor, P., Wernli, H., Hegglin, M. I., and Bönisch, H.: Transport timescales and tracer properties in the extratropical UTLS, Atmos. Chem. Phys., 10, 7929–7944, doi:10.5194/acp-10-7929-2010, 2010. 10598

Hsu, C. J. and Plumb, R. A.: Non-axisymmetric thermally driven circulations and upper tropospheric monsoon dynamics, J. Atmos. Sci., 57, 1254–1276, 2000. 10595

James, R., Bonazzola, M., Legras, B., Surbled, K., and Fueglistaler, S.: Water vapor transport and dehydration above convective outflow during Asian monsoon, Geophys. Res. Lett., 35, L20810, doi:10.1029/2008GL035441, 2008. 10595

Konopka, P., Günther, G., Müller, R., dos Santos, F. H. S., Schiller, C., Ravegnani, F., Ulanovsky, A., Schlager, H., Volk, C. M., Viciani, S., Pan, L. L., McKenna, D.-S., and Riese, M.: Contribution of mixing to upward transport across the tropical tropopause layer (TTL), Atmos. Chem. Phys., 7, 3285–3308, doi:10.5194/acp-7-3285-2007, 2007. 10597

Konopka, P., Grooß, J.-U., Günther, G., Ploeger, F., Pommrich, R., Müller, R., and Livesey, N.: Annual cycle of ozone at and above the tropical tropopause: observations versus simulations with the Chemical Lagrangian Model of the Stratosphere (CLaMS), Atmos. Chem. Phys., 10, 121–132, doi:10.5194/acp-10-121-2010, 2010. 10598

Krishnamurti, T. N., Daggupaty, S. M., Fein, J., Kanamitsu, M., and Lee, J. D.: Tibetan high and upper tropospheric tropical circulation during Northern summer, B. Am. Meteorol. Soc., 54, 1234–1249, 1973. 10595

ACPD
15, 10593–10628, 2015

Kunz, A., Konopka, P., Müller, R., and Pan, L. L.: Dynamical tropopause based on isentropic potential vorticity gradients, J. Geophys. Res., 116, D01110, doi:10.1029/2010JD014343, 2011. 10599, 10600, 10601, 10606

Kunze, M., Braesicke, P., Langematz, U., Stiller, G., Bekki, S., Brühl, C., Chipperfield, M., Dameris, M., Garcia, R., and Giorgetta, M.: Influences of the Indian summer monsoon on water vapor and ozone concentrations in the UTLS as simulated by chemistry-climate models, J. Climate, 23, 3525–3544, 2010. 10604

Livesey, N. J., Filipiak, M. J., Froideveaux, L., Read, W. G., Lambert, A., Santee, M. L., Jiang, J. H., Pumphrey, H. C., Waters, J. W., Cofield, R. E., Cuddy, D. T., Daffer, W. H., Drouin, B. J., Fuller, R. A., Jarnot, R. F., Jiang, Y. B., Knosp, B. W., Li, Q. B., Perun, V. S., Schwartz, M. J., Snyder, W. J., Stek, P. C., Thurstans, R. P., Wagner, P. A., Avery, M., Browell, E. V., Cammas, J. P., Christensen, L. E., Diskin, G. S., Gao, R. S., Jost, H. J., Loewenstein, M., Lopez, J. D., Nedelec, P., Osterman, G. B., Sachse, G. W., and Webster, C. R.: Validation of Aura Microwave Limb Sounder O_3 and CO observations in the upper troposphere and lower stratosphere, J. Geophys. Res., 113, D15S02, doi:10.1029/2007JD008805, 2008. 10598

McKenna, D. S., Grooß, J.-U., Günther, G., Konopka, P., Müller, R., Carver, G., and Sasano, Y.: A new Chemical Lagrangian Model of the Stratosphere (CLaMS): 2. Formulation of chemistry scheme and initialization, J. Geophys. Res., 107, 4256, doi:10.1029/2000JD000113, 2002a. 10597

McKenna, D. S., Konopka, P., Grooß, J.-U., Günther, G., Müller, R., Spang, R., Offermann, D., and Orsolini, Y.: A new Chemical Lagrangian Model of the Stratosphere (CLaMS): 1. Formulation of advection and mixing, J. Geophys. Res., 107, 4309, doi:10.1029/2000JD000114, 2002b. 10597

Nash, E. R., Newman, P. A., Rosenfield, J. E., and Schoeberl, M. R.: An objective determination of the polar vortex using Ertel's potential vorticity, J. Geophys. Res., 101, 9471–9478, 1996. 10594, 10595, 10597, 10599, 10600, 10605, 10606, 10608

Neu, J. L., Sparling, L. C., and Plumb, R. A.: Variability of the subtropical "edges" in the stratosphere, J. Geophys. Res., 108, 4482, doi:10.1029/2002JD002706, 2003. 10605

Palazzi, E., Fierli, F., Stiller, G. P., and Urban, J.: Probability density functions of long-lived tracer observations from satellite in the subtropical barrier region: data intercomparison, Atmos. Chem. Phys., 11, 10579–10598, doi:10.5194/acp-11-10579-2011, 2011. 10605

ACPD
15, 10593–10628, 2015

Park, M., Randel, W. J., Gettelman, A., Massie, S. T., and Jiang, J. H.: Transport above the Asian summer monsoon anticyclone inferred from Aura Microwave Limb Sounder tracers, J. Geophys. Res., 112, D16309, doi:10.1029/2006JD008294, 2006. 10595, 10605

Park, M., Randel, W. J., Emmons, L. K., Bernath, P. F., Walker, K. A., and Boone, C. D.: Chemical isolation in the Asian monsoon anticyclone observed in Atmospheric Chemistry Experiment (ACE-FTS) data, Atmos. Chem. Phys., 8, 757–764, doi:10.5194/acp-8-757-2008, 2008. 10595, 10605

Ploeger, F., Konopka, P., Müller, R., Fueglistaler, S., Schmidt, T., Manners, J. C., Grooß, J.-U., Günther, G., Forster, P. M., and Riese, M.: Horizontal transport affecting trace gas seasonality in the Tropical Tropopause Layer TTL, J. Geophys. Res., 117, 09303, doi:10.1029/2011JD017267, 2012. 10598

Ploeger, F., Günther, G., Konopka, P., Fueglistaler, S., Müller, R., Hoppe, C., Kunz, A., Spang, R., Grooß, J.-U., and Riese, M.: Horizontal water vapor transport in the lower stratosphere from subtropics to high latitudes during boreal summer, J. Geophys. Res., 118, 8111–8127, doi:10.1002/jgrd.50636, 2013. 10599

Pommrich, R., Müller, R., Grooß, J.-U., Konopka, P., Ploeger, F., Vogel, B., Tao, M., Hoppe, C. M., Günther, G., Spelten, N., Hoffmann, L., Pumphrey, H.-C., Viciani, S., D'Amato, F., Volk, C. M., Hoor, P., Schlager, H., and Riese, M.: Tropical troposphere to stratosphere transport of carbon monoxide and long-lived trace species in the Chemical Lagrangian Model of the Stratosphere (CLaMS), Geosci. Model Dev., 7, 2895–2916, doi:10.5194/gmd-7-2895-2014, 2014. 10598

Popovich, J. M. and Plumb, R. A.: Eddy shedding from the upper-tropospheric Asian Monsoon Anticyclone, J. Atmos. Sci., 58, 93–104, 2001. 10595

Randel, W. J. and Park, M.: Deep convective influence on the Asian summer monsoon anticyclone and associated tracer variability observed with Atmospheric Infrared Sounder (AIRS), J. Geophys. Res., 111, D12314, doi:10.1029/2005JD006490, 2006. 10595, 10596, 10597

Randel, W. J., Park, M., Emmons, L., Kinnison, D., Bernath, P., Walker, K. A., Boone, C., and Pumphrey, H.: Asian Monsoon transport of pollution to the stratosphere, Science, 328, 611–613, doi:10.1126/science.1182274, 2010. 10594

Sparling, L. C.: Statistical perspectives on stratospheric transport, Rev. Geophys., 38, 417–436, 2000. 10604

ACPD
15, 10593–10628, 2015

Tzella, A. and Legras, B.: A Lagrangian view of convective sources for transport of air across the Tropical Tropopause Layer: distribution, times and the radiative influence of clouds, Atmos. Chem. Phys., 11, 12517–12534, doi:10.5194/acp-11-12517-2011, 2011. 10594

Vogel, B., Günther, G., Müller, R., Grooß, J.-U., Hoor, P., Krämer, M., Müller, S., Zahn, A., and Riese, M.: Fast transport from Southeast Asia boundary layer sources to northern Europe: rapid uplift in typhoons and eastward eddy shedding of the Asian monsoon anticyclone, Atmos. Chem. Phys., 14, 12745–12762, doi:10.5194/acp-14-12745-2014, 2014. 10599

WMO: Meteorology – a three-dimensional science, WMO Bull., 6, 134–138, 1957. 10615

Yan, R.-C., Bian, J.-C., and Fan, Q.-J.: The impact of the South Asia high bimodality on the chemical composition of the upper troposphere and lower stratosphere, Atmos. Ocean. Sci. Lett., 4, 220–234, 2011. 10607

Zhang, Q., Wu, G., and Qian, Y.: The bimodality of the 100 hpa South Asia high and its relationship to the climate anomaly over East Asia in summer, J. Meteorol. Soc. Jpn., 80, 733–744, 2002. 10607

ACPD
15, 10593–10628, 2015

Table 1. Transport barrier PV values for the Asian monsoon anticyclone at 380 K calculated from maximum PV and CO gradients and maximum-minimum ranges for the years 2011–2013 (averages over all dates between 20 June and 20 August of each year where the transport barrier criterion holds).

	2011	2012	2013
PV–barrier/PVU	3.6 (3.0–4.4)	3.8 (2.6–4.4)	3.5 (2.6–4.4)
CO–barrier/PVU	3.7 (3.2–4.4)	3.7 (2.4–4.6)	3.6 (2.6–4.2)

ACPD
15, 10593–10628, 2015

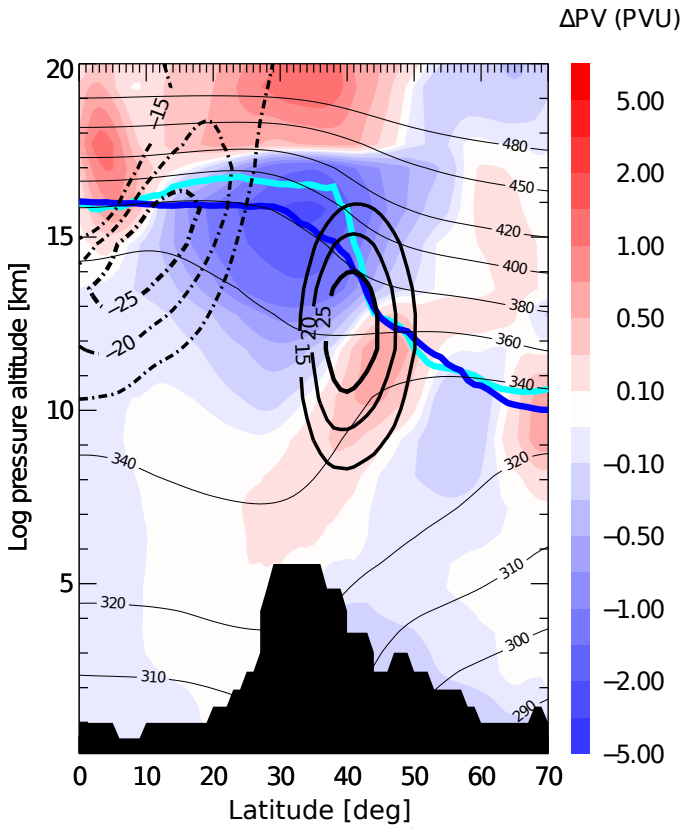

Figure 1. Meteorological conditions in the Asian monsoon anticyclone. Color shading shows the PV anomaly of the monsoon longitude section (60–120° E) with respect to the zonal mean, averaged over summer (June–August). Also shown is zonal wind (thick black, solid/dashed positive/negative) and potential temperature (thin black) averaged between 60–120° E. The first thermal tropopause (calculated using the definition of WMO, 1957) zonally averaged over 0–360° E is shown as dark-blue, averaged over 60–120° E as cyan line.

ACPD
15, 10593–10628, 2015

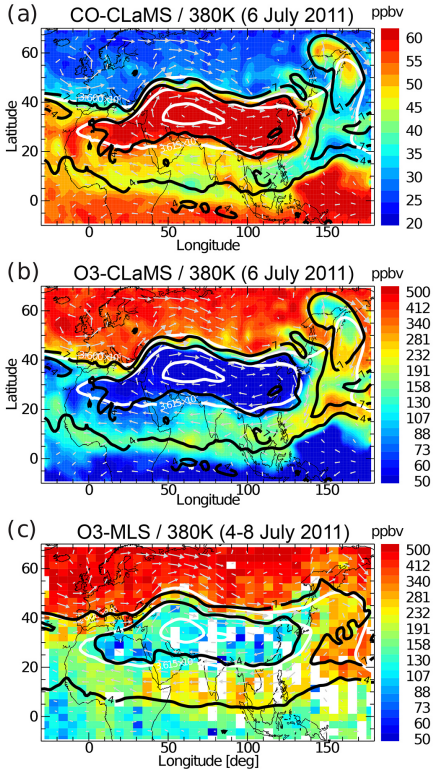

Figure 2. Maps of **(a)** CLaMS CO and **(b)** CLaMS ozone on the 380 K isentrope on 6 July 2011 within the Asian monsoon region. Selected potential vorticity contours are shown in black (4, 7 PVU) and Montgomery stream function contours in white (3.6×10^5, 3.615×10^5 $m^2 s^{-2}$). Arrows show horizontal wind. **(c)** Same but for MLS ozone during the period 4–8 July 2011, with the MLS data binned into 3° × 6° latitude/longitude bins (bins without measurements are left white). Meteorological data is taken from ERA-Interim. (Note the logarithmic color scale for ozone.)

ACPD
15, 10593–10628, 2015

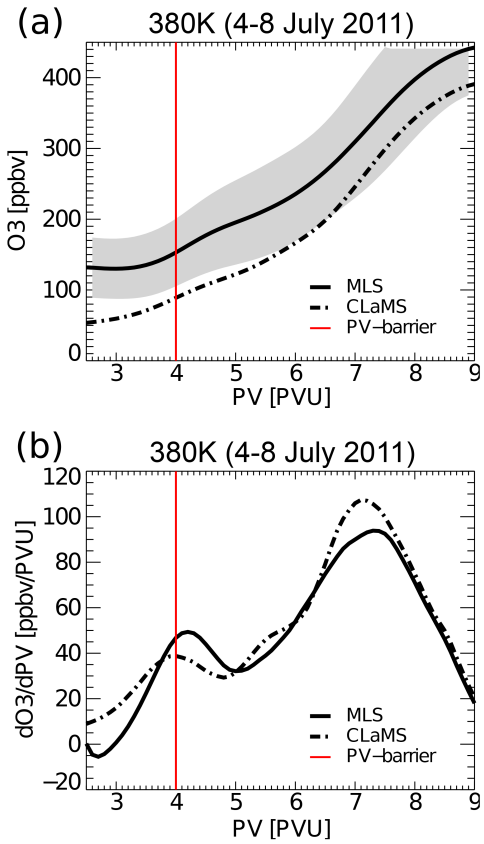

Figure 3. (a) Ozone from MLS (solid) and CLaMS (dashed) vs. potential vorticity in the Asian monsoon region (10–60° N and 10° W–160° E) at 380 K, averaged over the period 4–8 June 2011. **(b)** Same but for the ozone gradient with respect to potential vorticity. Red lines show the transport barrier determined from PV (see text).

ACPD
15, 10593–10628, 2015

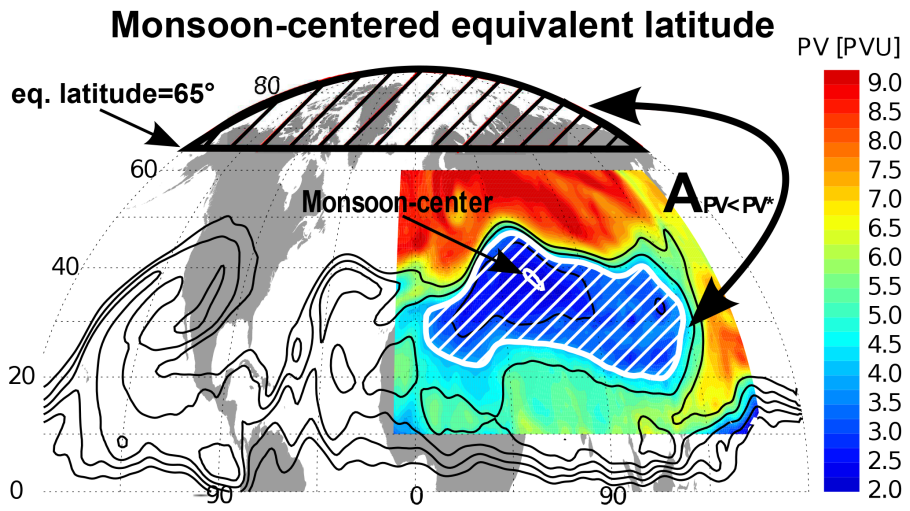

Figure 4. Illustration of the calculation of monsoon-centered equivalent latitude from the area within PV-contours (see text for details). Color-coded is the PV-field within the Asian monsoon region (10–60° N and 10° W–160° E) averaged for 5–7 July 2011, with the white contour highlighting 4 PVU. The black contours show PV globally.

ACPD
15, 10593–10628, 2015

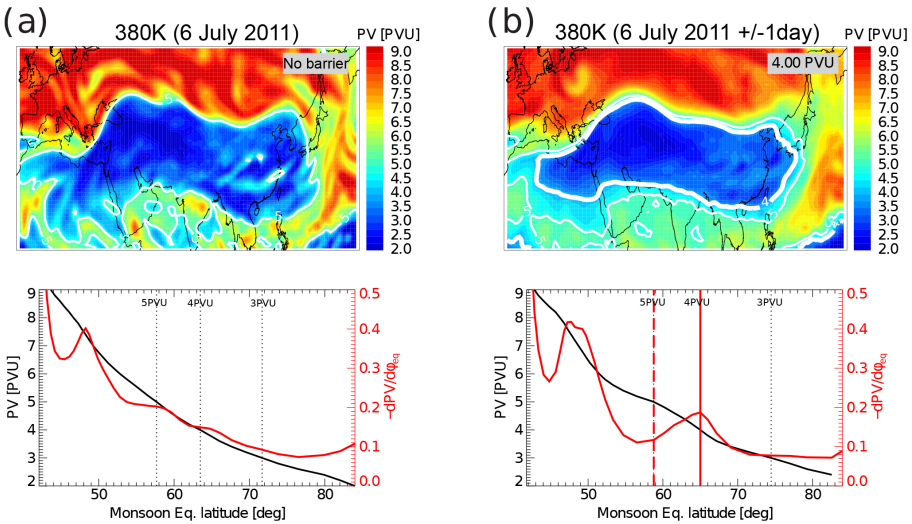

Figure 5. (a) Potential vorticity map at 380 K on 6 July 2011, in the Asian monsoon region between 10–60° N and 10° W–160° E (upper panel), and PV as function of the monsoon centered equivalent latitude (lower panel). Monsoon equivalent latitude ϕ_{eq} is calculated from the area within PV contours (see text). Shown is PV(ϕ_{eq}) (black) together with the respective PV gradient $\partial PV/\partial\phi_{eq}$ (red). Low PV and large ϕ_{eq} indicate the anticyclone center. **(b)** Same as **(a)** but for the PV-field averaged between 5 and 7 July 2011. The anticyclone transport barrier, deduced from the maximum PV gradient (see text), is shown as white thick contours (upper panels) and red solid vertical lines (lower panels), respectively. White thin contours (upper panels) and red dashed lines (lower panels) show 5 PVU. Black dashed lines (lower panels) highlight particular PV values. The PV value of the barrier is given in the grey box.

ACPD
15, 10593–10628, 2015

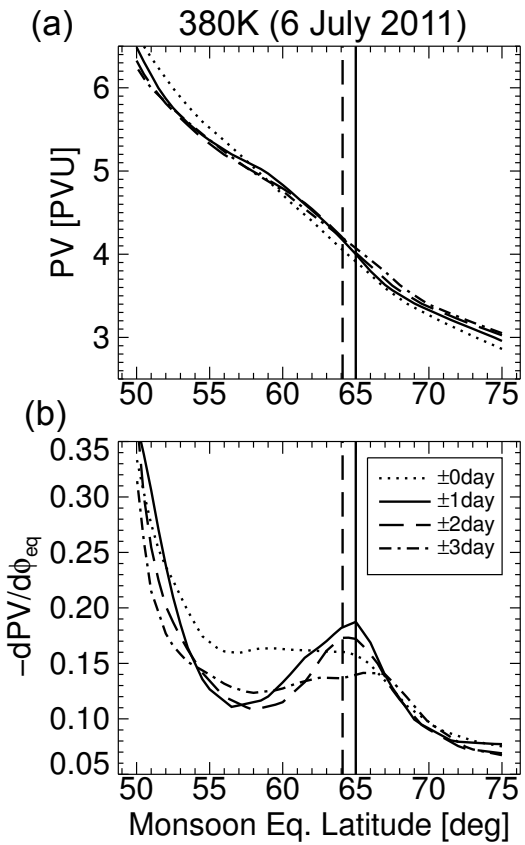

Figure 6. (a) Potential vorticity with respect to monsoon centered equivalent latitude on the 380 K isentrope, with the PV field averaged over different periods centered around 6 July 2011. **(b)** The corresponding gradients of PV with respect to equivalent latitude. Vertical lines show the PV-gradient maximum.

ACPD
15, 10593–10628, 2015

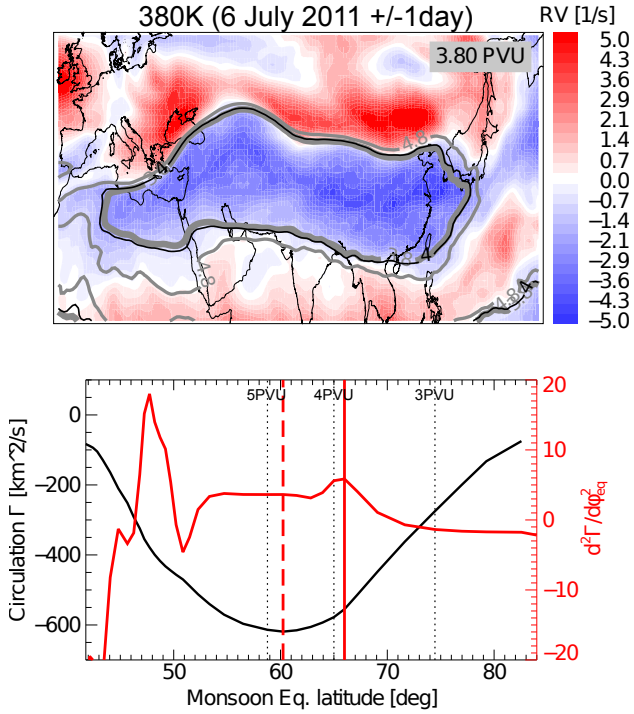

Figure 7. Relative vorticity map at 380 K, in the Asian monsoon region between 10–60° N and 10° W–160° E averaged over 5–7 July 2011 (upper panel). The lower panel shows the horizontal circulation (calculated from area-integrated relative vorticity) as function of the monsoon centered equivalent latitude (black) and the respective second derivative (red). PV values corresponding to the minimum circulation are shown as thin grey contour (upper panel) and red dashed line (lower), and PV values corresponding to the maximum in the second derivative of the circulation as thick grey contour (upper) and red solid line (lower). The black contour (upper panel) shows the transport barrier PV deduced from the maximum PV-gradient, for comparison. (See text for further details.)

ACPD
15, 10593–10628, 2015

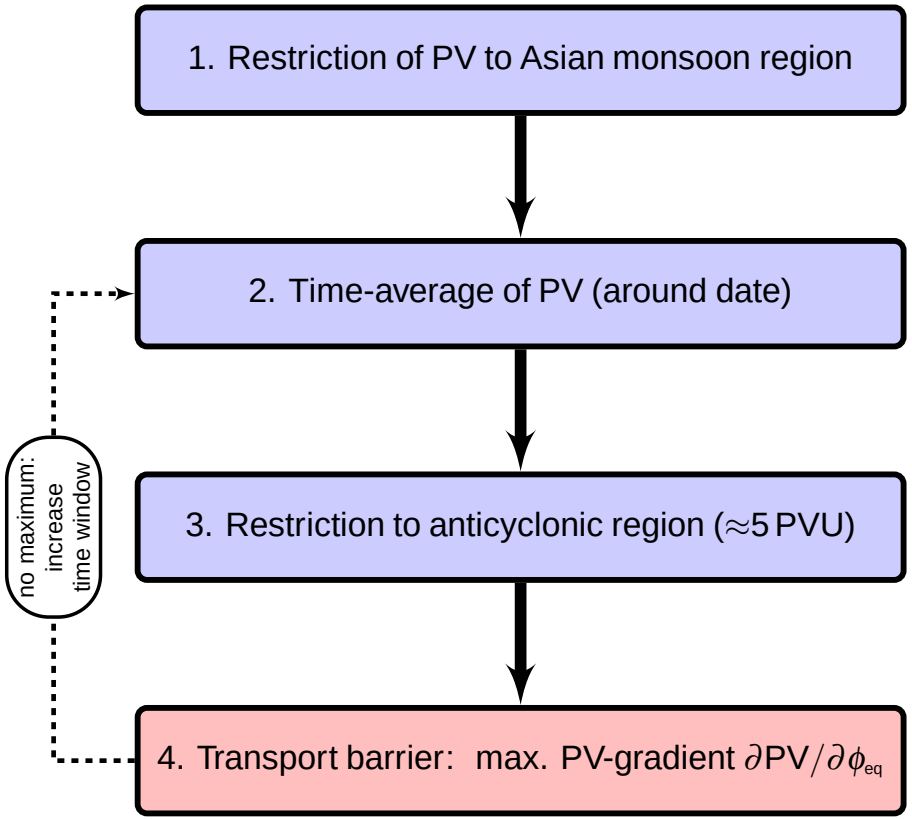

Figure 8. Method to localize the PV-based transport barrier in the Asian monsoon anticyclone (at 380 K), summarized in four steps.

ACPD
15, 10593–10628, 2015

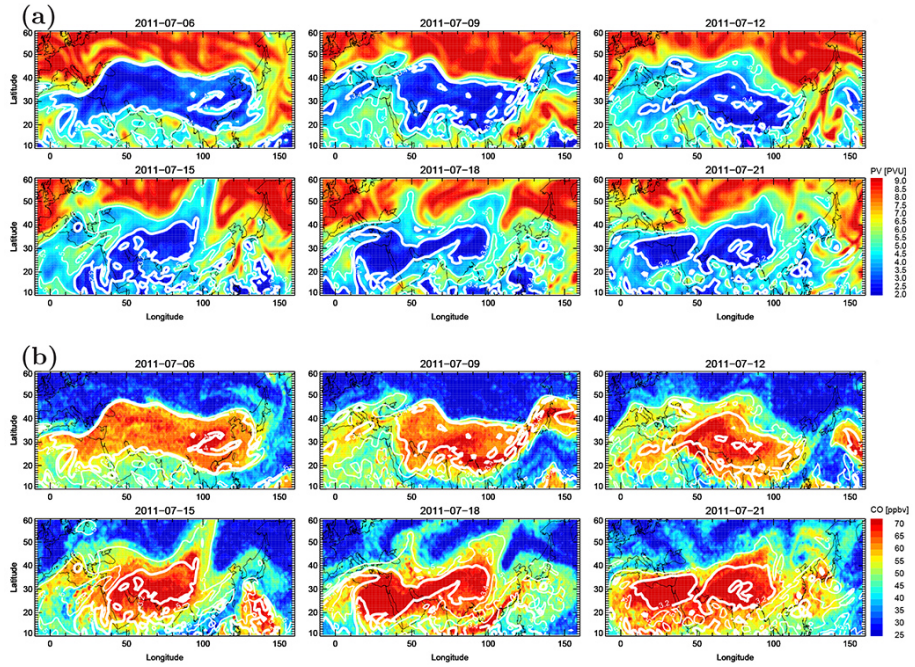

Figure 9. (a) Potential vorticity maps at 380 K on 6/9/12/15/18/21 July 2011. The thick white contour shows the calculated anticyclone transport barrier (maximum PV gradient), the thin white contour 5 PVU. **(b)** Maps of CO from CLaMS on the same days, with PV-based transport barrier included as white contours.

ACPD
15, 10593–10628, 2015

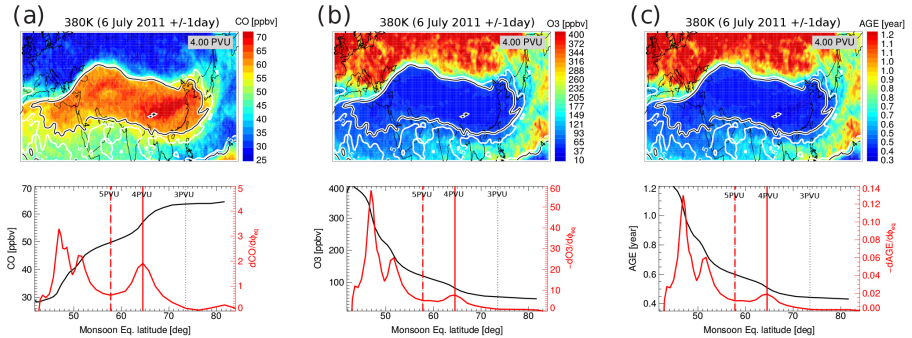

Figure 10. (a) Map of CO from CLaMS on the 380 K isentrope, with the thick white contour showing the PV value of maximum CO-gradient, the black contour showing the PV value of maximum PV-gradient (thin white line shows 5 PVU), averaged between 5 and 7 July 2011 at 380 K. The bottom panel shows CO from CLaMS vs. monsoon centered equivalent latitude (black), and the respective gradient (red). **(b)** Same for ozone from CLaMS, and **(c)** for mean age from CLaMS. (The PV values of the maximum gradient are given in the upper panels.)

ACPD
15, 10593–10628, 2015

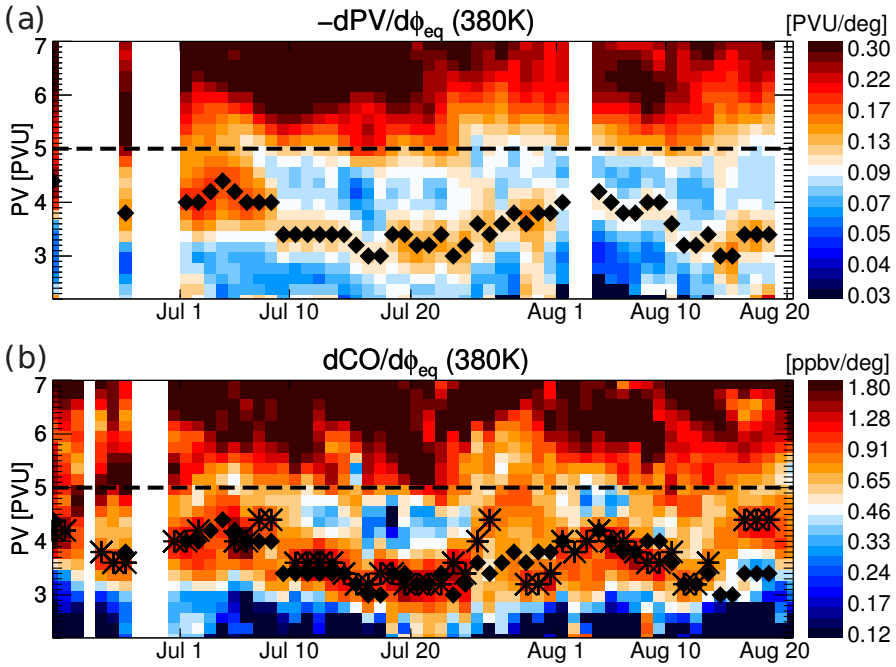

Figure 11. (a) Time evolution of the gradient of PV with respect to monsoon centered equivalent latitude ϕ_{eq} as a function of PV for June–August 2011 at 380 K (note the logarithmic color scale). **(b)** Same but for CO. Black symbols show the PV-gradient maximum (diamonds), and the CO-gradient maximum (crosses). The dashed line highlights 5 PVU. Dates without a clear gradient maximum are left white.

ACPD
15, 10593–10628, 2015

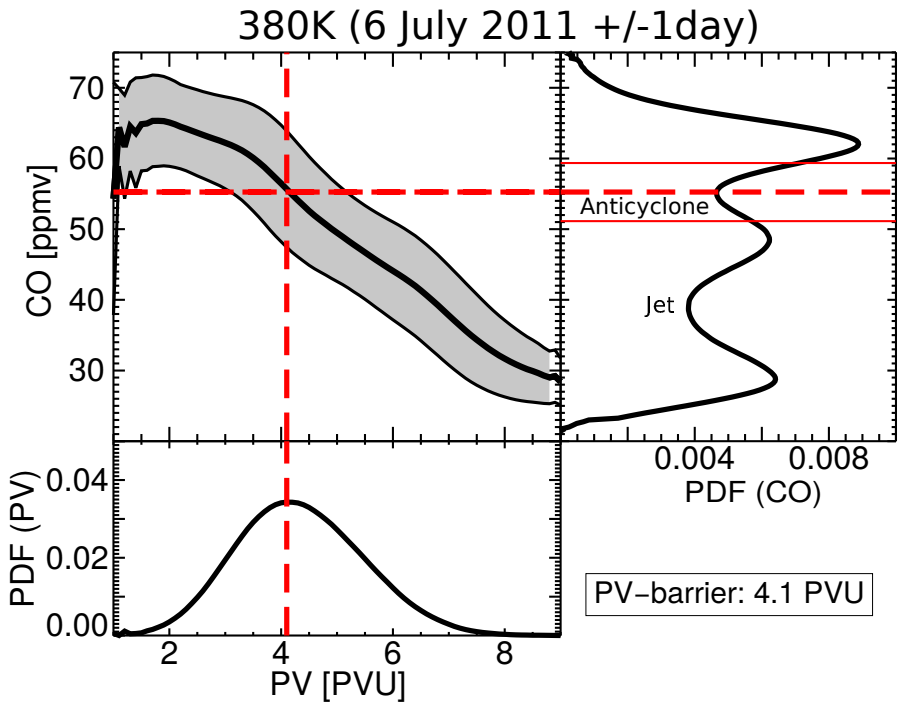

Figure 12. Asian monsoon transport barrier at 380 K on 6 July 2011 from CO mixing ratio PDF. Shown is CLaMS CO (monsoon region average, 5–7 July time average) vs. PV with one standard deviation as grey shading (upper left panel), and the corresponding mixing ratio PDF with the monsoon transport barrier highlighted as red dashed line (upper right). The lower panel shows the PDF of PV values around the barrier (between the thin red lines in upper right panel). (See text for further details.)

ACPD
15, 10593–10628, 2015

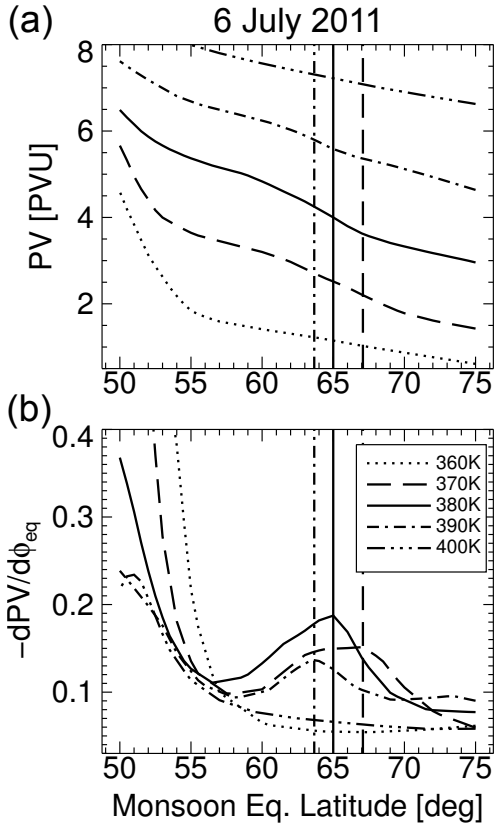

Figure 13. (a) Potential vorticity with respect to monsoon centered equivalent latitude on 6 July 2011, on different levels (360, 370, 380, 390, 400 K isentropes). **(b)** The corresponding PV-gradients with respect to equivalent latitude. Vertical lines show the gradient maxima (transport barriers).

ACPD
15, 10593–10628, 2015

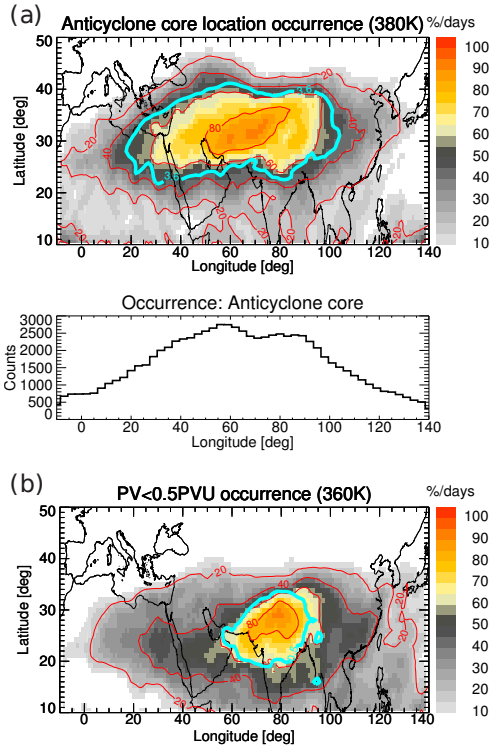

Figure 14. (a) Occurrence frequency of the Asian monsoon anticyclone at 380 K (in percentage of days) for the period between 20 June and 20 August 2011, calculated from the area covered by PV values lower than the anticyclone transport barrier. Red contours show selected percentage values, the thick cyan contour shows the average PV value of the barrier in the average PV field (average over period considered). The bottom panel shows the projection of anticyclone occurrence frequency onto the longitude axis (bin size 2.5°). **(b)** Occurrence frequency for PV values below 0.5 PVU at 360 K isentrope, for the same period.

ACPD
15, 10593–10628, 2015